Effect of Local DBD Plasma Actuation on Transition in a Laminar Separation Bubble

Yarusevych, Serhiy; Kotsonis, Marios

DOI
10.1007/s10494-016-9738-1

Publication date
2017

Document Version
Final published version

Published in
Flow, Turbulence and Combustion

Flow Turbulence Combust (2017) 98:195–216
DOI 10.1007/s10494-016-9738-1

Effect of Local DBD Plasma Actuation on Transition in a Laminar Separation Bubble

Serhiy Yarusevych[1] · **Marios Kotsonis**[2]

Received: 15 November 2015 / Accepted: 30 March 2016 / Published online: 17 May 2016

Abstract This work examines the effect of local active flow control on stability and transition in a laminar separation bubble. Experiments are performed in a wind tunnel facility on a NACA 0012 airfoil at a chord Reynolds number of 130 000 and an angle of attack of 2 degrees. Controlled disturbances are introduced upstream of a laminar separation bubble forming on the suction side of the airfoil using a surface-mounted Dielectric Barrier Discharge plasma actuator. Time-resolved two-component Particle Image Velocimetry is used to characterise the flow field. The effect of frequency and amplitude of plasma excitation on flow development is examined. The introduction of artificial harmonic disturbances leads to significant changes in separation bubble topology and the characteristics of coherent structures formed in the aft portion of the bubble. The development of the bubble demonstrates strong dependence on the actuation frequency and amplitude, revealing the dominant role of incoming disturbances in the transition scenario. Statistical, topological and linear stability theory analysis demonstrate that significant mean flow deformation produced by controlled disturbances leads to notable changes in stability characteristics compared to those in the unforced baseline case. The findings provide a new outlook on the role of controlled disturbances in separated shear layer transition and instruct the development of effective flow control strategies.

Keywords Laminar separation bubble · Airfoil · Boundary layer separation · Separated shear layer · Laminar-to-turbulent transition · DBD plasma actuator · Flow control

✉ Serhiy Yarusevych
syarus@uwaterloo.ca

[1] Department of Mechanical and Mechatronics Engineering, University of Waterloo, 200 University Ave. W, Waterloo, Ontario N2L 3G1, Canada

[2] Faculty of Aerospace Engineering, Delft University of Technology, Kluyverweg 1, 2629 HS Delft, The Netherlands

1 Introduction

A Laminar Separation Bubble (LSB) is a characteristic feature of flow development over airfoils at low chord Reynolds numbers (Re_c) [1]. It typically forms on the suction side of an airfoil due to laminar boundary layer separation, followed by separated shear layer transition and subsequent reattachment in turbulent state. In general, the airfoil performance degrades in the low Reynolds number domain, and the degree of performance degradation largely depends on the characteristics of the laminar separation bubble [1, 2]. Consequently, significant research efforts have been directed towards gaining an improved understanding of flow phenomena within separation bubbles [3–7] and developing effective flow control strategies [8–11].

Early studies of laminar separation bubbles [2, 12] have provided a comprehensive description of the time-averaged separation bubble topology. Subsequently, significant advancements have been made towards a comprehensive characterisation of separated shear layer transition [4, 7, 13–15]. It has been shown that the transition process begins with the amplification of small amplitude disturbances in the separated shear layer. The initial amplification is associated with a band of unstable frequencies and is well modelled by Linear Stability Theory (LST). The process is largely governed by a convective, inviscid Kelvin-Helmholtz instability. However, Alam & Sandham [16] have demonstrated that an absolute instability can also manifest in the separated shear layer when it is bound by a strong reverse flow region near the wall. This requires maximum reverse flow velocities to reach approximately 15% of the edge velocity, which is uncommon in separation bubbles investigated experimentally. The later stages of transition in the separated shear layer involve non-linear interaction between the disturbances, and the continuous growth of disturbance amplitude leads to separated shear layer roll-up and shedding of shear layer vortices in the aft portion of the bubble [17, 18]. These structures are argued to be responsible for producing time-averaged flow reattachment [3, 7]. Yarusevych et al. [19, 20] suggest that the roll-up vortices are shed periodically at the frequency of the most amplified disturbances in the shear layer, which is supported by numerical simulations in [7, 17, 18]. The shear layer vortices are observed to undergo significant deformation and begin to break down in the aft portion of the bubble [3, 17, 18, 21].

The key role played by the transition process in the development of separation bubbles makes these flows sensitive to background disturbances in experimental facilities [22] and numerical simulations [7]. It also enables the implementation of active flow control strategies that can impact LSB characteristics and improve airfoil performance. Periodic excitation using external acoustic waves [11], embedded synthetic jets [23], and plasma-based actuators [24] have been considered and shown to be capable of inducing flow reattachment on an airfoil exhibiting separation. The effectiveness of the control depends strongly on the amplitude and the frequency of excitation. Using controlled acoustic excitation, Yarusevych et al. [11] have identified a link between the most effective excitation frequency and that of the most amplified disturbances in undisturbed flow. Marxen & Henningson [7] and Marxen et al. [9] considered the effect of controlled disturbances on the development of a separation bubble in direct numerical simulations. Their results show that the introduction of flow perturbations changes the topology of the bubble, implying that flow excitation also influences stability characteristics of the time-averaged laminar separation bubble. LST analysis performed on numerical results in [9] shows reduction of the frequency of the most amplified disturbances due to mean flow deformation, compared to the non-actuated baseline case. The reduction in the size of the bubble was also observed to be accompanied by the reduction in the maximum growth rate. The authors

suggest that different control mechanisms can be at play at different excitation frequencies. However, the most efficient in the reduction of the separation bubble is the forcing applied at the frequency of the most amplified linear stability mode, adjusted for the mean flow deformation effects. These findings, however, are yet to be confirmed in an experiment.

The present work investigates experimentally the response of LSBs to local disturbances. The goal is to investigate the spatio-temporal response of the bubble to controlled disturbances and to study the effect of the associated changes in the flow topology on stability and transition in the separated shear layer. This is accomplished by means of time-resolved, planar, two-component Particle Image Velocimetry (PIV) measurements that effectively capture the two-dimensional spatio-temporal dynamics of the separation bubble. The amplitude and spectral content of the introduced disturbances are deterministically controlled using a Dielectric Barrier Discharge (DBD) plasma actuator. Proper Orthogonal Decomposition (POD) and linear stability analysis of experimental data are employed to elucidate the changes to the most energetic modes and stability characteristics produced by the controlled excitation of the flow.

2 Experimental Setup

The experiments were performed in the vertical, low-speed open-jet facility (v-tunnel) at Delft University of Technology. The wind tunnel is capable of maximum velocities of 40 m/s, while a large contraction ratio of 100:1 and anti-turbulence screens ensure freestream turbulence levels below 0.1 %. A polycarbonate NACA-0012 airfoil model, with a chord length of 200 mm and a span of 400 mm, was placed about 150 mm downstream of a circular open-jet nozzle (diameter of 600 mm) (Fig. 1). Circular, transparent polycarbonate side plates of diameter 300 mm were used to mitigate any end effects while allowing for optical access. The end plates were spaced by two airfoil chords based on the recommendations provided in [25]. The boundary layer on the pressure side of the airfoil was tripped using a strip of randomly distributed three-dimensional roughness elements (carborundum, nominal grain size of 0.36 mm). This was done in order to prevent the formation of a separation bubble on the pressure side of the airfoil and the associated shedding of coherent structures over the trailing edge, which can produce tonal noise emissions and affect the dynamics of the LSB on the suction side [26]. All experiments were conducted at a freestream velocity $U_\infty = 10m/s$, corresponding to a chord Reynolds number of approximately 130 000.

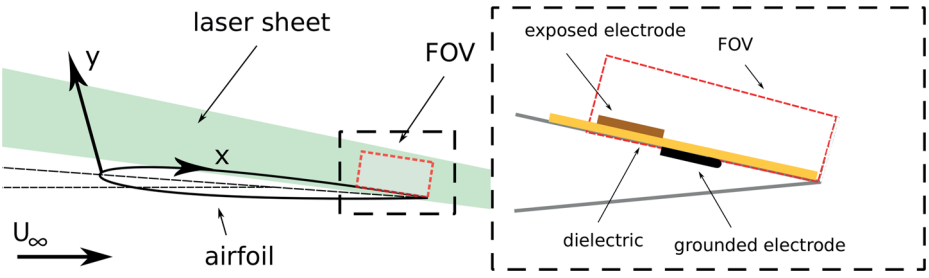

Fig. 1 Experimental setup and detail in the vicinity of the PIV field-of-view. Plasma actuator is not drawn to scale. Origin of the surface-attached coordinate system is located at the airfoil leading edge

Time-resolved, planar, two-component PIV measurements were performed with a system comprised of a LaVision Imager Pro HS 4M high speed CMOS camera, with a maximum resolution of 4 million pixels and $11\mu m$ pixel pitch. The domain of interest was illuminated by a dual-pulse Quantronix Darwin-Duo Nd:YLF laser (maximum energy of 30 mJ per pulse). The camera and the laser were synchronised with a LaVision High-Speed controller, and images were acquired using Davis 8 software package. The flow was seeded using non-toxic, water-glycol particles with an average diameter of $1\mu m$. The particles were illuminated at the mid-span of the airfoil model by a light sheet of approximately 2 mm in thickness. The camera was equipped with a Nikon Micro-Nikkor 105 mm objective with aperture number ($f\#$) set to 5.6. The imaged field of view (FOV) was approximately 90 x 19 mm, with a magnification factor of approximately 0.25. The camera sensor was cropped to 2016 x 428 pixels and image pairs were recorded at 2 kHz in double-frame mode. The acquired image sequences were analysed using a multi-grid, multi-pass correlation algorithm in Davis 8. The final interrogation window size was 16 x 16 pixels, with 75% overlap, resulting in a vector density of 5.6 vectors per mm. Uncertainty quantification is applied to the instantaneous vector fields using the technique of Wieneke [27], implemented in Davis 8. The estimated uncertainty in time-averaged velocity fields due to random errors (maximum value of $0.04U_\infty$ in the reattachment region) is used for the estimation of uncertainties associated with the identification of the dividing streamline, separation and reattachment points, and integral boundary layer lengths pertaining to each case investigated.

A surface-attached coordinate system is used for data presentation (Fig. 1). The x-axis originates at the leading edge and is measured along the suction side of the airfoil; whereas, the y-axis is measured normal and relative to the airfoil surface at a given x location. It must be noted that planar PIV inherently provides two-dimensional velocity measurements. This can sufficiently resolve the initial growth of coherent structures in the separated shear layer but not the strong three-dimensional events known to develop in the aft portion of LSBs. These events are associated with the non-linear development and breakdown of the roll-up vortices [28]. Considering this, the observations and conclusions of this study are focused on the time-average flow characteristics, initial growth and spatio-temporal development of coherent structures. Description of the flow near and downstream of reattachment is restricted to statistical values in order to minimise the effect of three-dimensionality.

Flow control was performed by means of a DBD plasma actuator. The actuator was directly attached on the surface of the suction side of the airfoil (Fig. 1) and comprised of two thin, self-adhesive copper electrodes of 30 μm thickness, separated by adhesive polyimide dielectric (Kapton) of 110 μm thickness. Comparison of PIV measurements with and without plasma actuator installed on the airfoil showed no appreciable effect of actuator-related roughness on the development and characteristics of the formed LSB. The exposed electrode was powered using a TREK 20/20C High-Voltage (HV) amplifier, while the covered electrode was grounded. Both electrodes were 10 mm wide in the streamwise direction and 120 mm in the spanwise direction. The actuator was placed 120 mm from the leading edge (at $x/c = 0.6$), just upstream of the mean laminar boundary layer separation point. Characterisation of the plasma actuator was performed in quiescent environment using time-resolved PIV. Representative mean and root-mean-square (rms) streamwise velocity profiles are presented in Fig. 2, pertaining to continuous excitation at carrier frequency of 5000 Hz and applied voltage of 5 kV_{pp}. In agreement with Kotsonis et al. [29], the actuator produces a wall-tangent micro-jet, oriented from the exposed to the covered electrode. Additionally, weak negative mean velocity is evident near the top of the measurement domain ($y/c > 0.02$), underlying a large recirculation area in the quiescent environment due to the

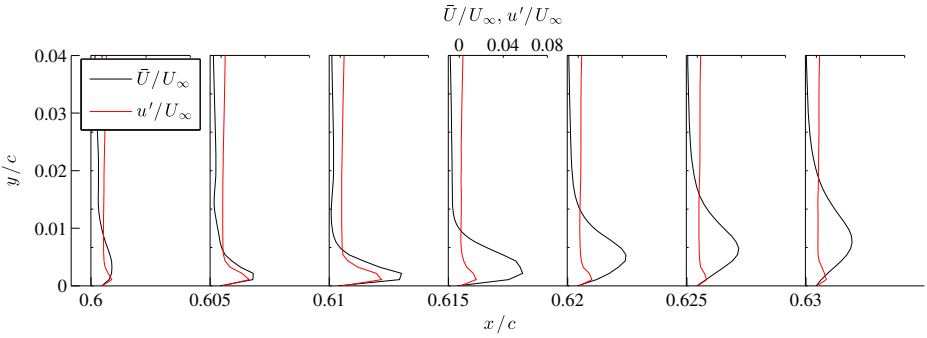

Fig. 2 Mean ($\bar{U}$) and rms (u') profiles of plasma induced velocity in quiescent conditions. The actuator is located at $x/c = 0.6$ and operated at amplitude of 5 kV_{pp} and carrier frequency of 5 kHz

near-wall jet. The velocity of the jet fluctuates periodically at the applied voltage frequency, producing perturbations captured in the rms profiles.

The actuator electrodes are positioned in a linear fashion along the spanwise direction. As such, the plasma-induced forcing, and in consequence the introduced flow perturbations, can be considered purely two-dimensional. Due to the importance of three-dimensional effects in the breakdown region of LSB, the results of this study can be considered to pertain only to two-dimensional upstream forcing. Cases of three-dimensional or spanwise modulated forcing are expected to differ significantly, as demonstrated by Marxen & Henningson [7] and Jones et al. [17].

In the present study, the plasma actuator was operated at an AC carrier frequency of 5 kHz, which is one order of magnitude higher than the highest frequency of interest in the flow investigated. In order to deterministically introduce disturbances at relevant hydrodynamic time scales, square wave modulation of the excitation voltage was applied at a desired frequency (effectively switching the actuator on and off). The modulation was applied at frequency (f) from 100 Hz to 500 Hz (corresponding to a reduced frequency $f^+ = fc/U_\infty$ ranging from 2 to 10, respectively). The frequency range was selected to correspond to a range of unstable frequencies naturally present in the undisturbed separation bubble. The amplitude of excitation was varied from 3 kV_{pp} to 5 kV_{pp}. Additionally, for a given voltage amplitude, the duty cycle was adjusted for each modulation frequency in order to yield the same energy input per pulse across the investigated range of frequencies. The excitation amplitude was characterised using a momentum coefficient ($c_\mu = J/q_\infty c$, where J is the total momentum of the jet induced by the plasma actuator in quiescent environment, q_∞ is the free stream dynamic pressure, and c is the airfoil chord). The momentum coefficient was characterised using direct force measurements performed on a high-precision force balance

Table 1 Plasma actuator momentum coefficient as function of voltage amplitude

A (kV_{pp})	c_μ
2	2.1×10^{-10}
2.5	2.0×10^{-9}
3	1.2×10^{-8}
3.5	5.8×10^{-8}
4	2.2×10^{-7}
5	2.0×10^{-6}

[29]. Due to the extremely low values of plasma-produced momentum at the tested voltage amplitudes (below the force balance resolution), higher voltage amplitudes were used for the calculation of the momentum coefficient. The values corresponding to the tested excitation amplitudes were then estimated using a power-law fit to the measured data [30] and are presented in Table 1.

3 Results

All the experimental data presented here were obtained at angle of attack $\alpha = 2°$ and Re_c =130 000. The parametric tests considered the response of the laminar separation bubble to controlled disturbances in a range of excitation amplitudes and frequencies around the natural frequency of the most amplified disturbances in an unperturbed flow.

Figure 3 illustrates the effect of excitation frequency ($f^+ = fc/U_\infty$) on time-averaged flow field characteristics. For the baseline case (no actuation), the results show the presence of a laminar separation bubble on the suction side of the airfoil. The bubble extends from $x/c = 0.62$ to $x/c = 0.97$. When disturbances are introduced at a constant actuation amplitude of 3.5 kV_{pp}, the extent of the bubble is notably diminished; however, the effect depends significantly on the excitation frequency. For the excitation applied continuously at the carrier frequency (5000 Hz), a moderate decrease in bubble length is observed, with both separation and reattachment locations being affected. At these operation settings, the actuator is perturbing the flow at a frequency significantly separated from the natural shedding frequency of the bubble. Thus, the effect on the separation bubble is attributed to the mean

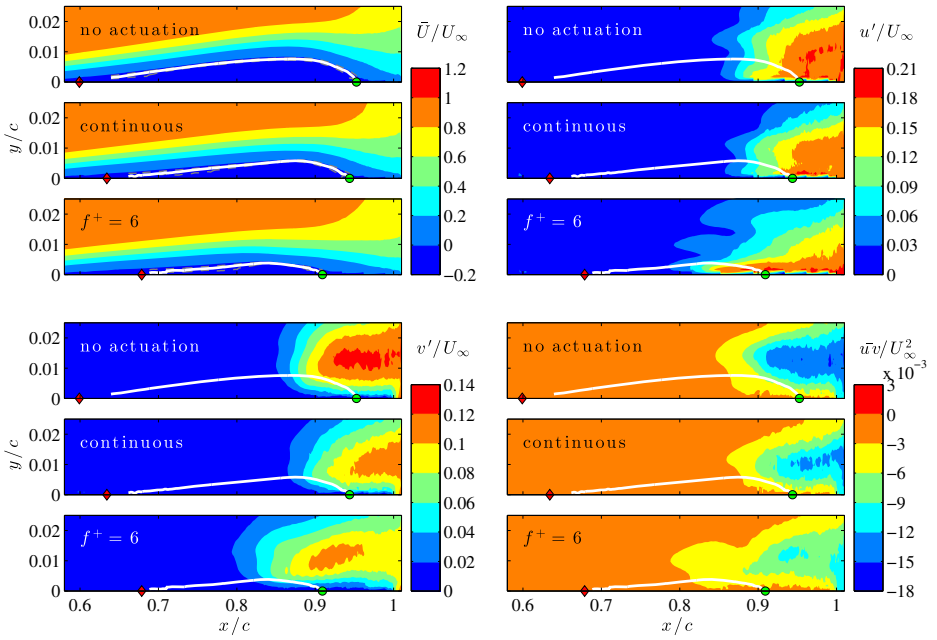

Fig. 3 Mean ($\bar{U}$) and rms (u', v') velocity contours, and Reynolds stress ($\bar{u}\bar{v}$) contours. For the controlled cases, the actuation is applied at 3.5 kV_{pp}. Solid white lines mark the dividing streamlines. Red diamonds denote the separation points while green circles denote the reattachment points

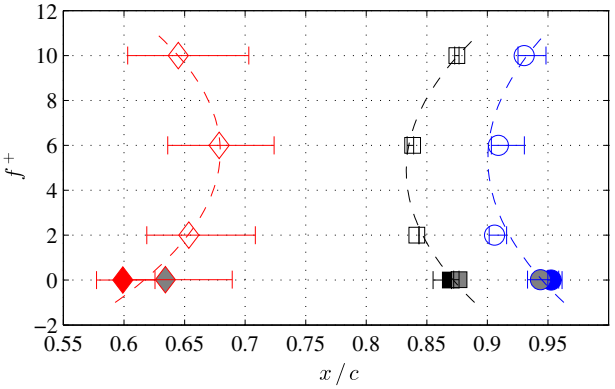

Fig. 4 The effect of excitation frequency on the location of laminar separation (*red diamonds*), maximum bubble height (*black squares*), and reattachment (*blue circles*). Solid symbols denote baseline case while grey symbols denote continuous actuation. All forced cases pertain to $A = 3.5kV_{pp}$ (fitted trend lines are second-order polynomials). Error bars denote uncertainty interval

injection of momentum by the actuator [30], primarily delaying boundary layer separation. However, the effect of actuation becomes more pronounced when the actuator is modulated at lower frequencies, e.g., at $f^+ = 6$ ($f = 300Hz$), which falls within the frequencies of the naturally amplified disturbances in the separated shear layer. Indeed, the contours of rms streamwise and vertical fluctuating velocity components show that the observed changes in the position and extent of the separation bubble are linked to the increase in the amplitude of disturbances in the separated shear layer, with velocity fluctuations attaining notably higher amplitudes at a given streamwise location when excitation is applied at $f^+ = 6$. As expected, a similar increase is seen in Reynolds stress, which is often used to track the location of transition in the separated shear layer [22]. The implication here is that actuation at $f^+ = 6$ advances transition in the separated shear layer, which not only induces earlier time-averaged reattachment but also delays separation by inducing significant changes in time-averaged parameters of the separation bubble.

The effect of excitation frequency on mean bubble characteristics is illustrated in Fig. 4, with all excitation cases pertaining to a constant excitation amplitude of $A = 3.5kV_{pp}$. The results indicate that the bubble reaches its minimum extent at $f^+ \approx 6$, suggesting the existence of optimal excitation frequency. A comparison of integral boundary layer parameters

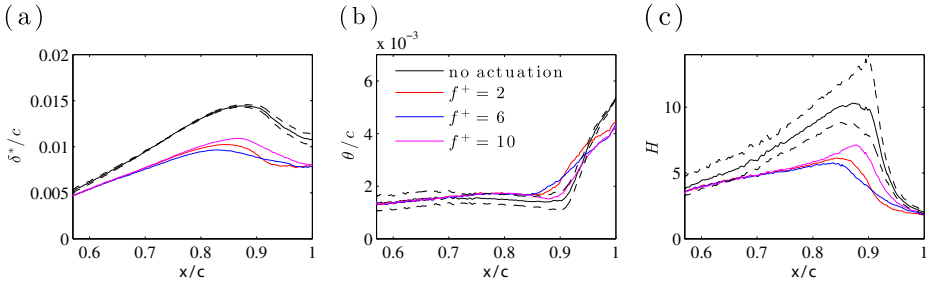

Fig. 5 Integral shear layer parameters for different excitation frequencies at $A = 3.5kV_{pp}$: **a** displacement thickness (δ^*), **b** momentum thickness (θ), **c** shape factor ($H = \delta^*/\theta$). Black dashed lines denote uncertainty for the no actuation case

presented in Fig. 5 shows that excitation of the flow at frequencies around $f^+ = 6$ leads to a significant decrease in displacement thickness (δ^*) and shape factor (H). In contrast, the momentum thickness (θ) in the fore portion of the bubble is not being affected significantly. Due to low reverse flow velocities in this region (Fig. 3), the skin friction is expected to be low and will not change appreciably, resulting in approximately constant momentum thickness until transition. The later stages of transition are marked by a steep increase in the momentum thickness and a decrease in displacement thickness, the latter attributed to flow reattachment in the time-averaged sense. Thus, the later stages of transition correspond to a distinct maximum in the shape factor, whose streamwise location approximately corresponds to that of the maximum bubble height (cf. Figs. 4 and 5). To assess the effect of excitation amplitude on separation bubble characteristics, the excitation was applied at a fixed frequency $f^+ = 6$. The results are summarised in Fig. 6, showing that the increase in excitation amplitude leads to a continuous diminishment of the separation bubble, with separation being delayed and reattachment occurring farther upstream. It should be noted that this effect is observed only once the amplitude exceeds a minimum threshold level. The observed effect of excitation amplitude on the characteristics of the separation bubble is similar to that reported by Yarusevych et al. [11] for external acoustic excitation.

The spectral content of disturbances amplified in the separated shear layer can be assessed using the power spectral density (PSD) profiles of streamwise velocity fluctuations shown in Fig. 7. For the baseline case, the packet of amplified disturbances is seen at frequencies within approximately $2 < F^+ < 10$. Evidently, the optimal excitation frequency $f^+ = 6$ identified in Fig. 4 is associated with the frequency of the most amplified disturbances in the baseline flow, where disturbances at $F^+ \approx 6$ reach higher amplitudes at a given streamwise location (Fig. 7). When the flow is excited at a given frequency, the spectral results show that the frequency of the most amplified disturbances in the shear layer locks to the excitation frequency and its harmonics. The most profound amplification is attained, however, when the excitation frequency (or its harmonic) matches that of the most unstable disturbances in the undisturbed flow. This leads to significant changes in separation bubble characteristics seen in Figs. 3–5. The results also illustrate the significance of harmonics amplification when such harmonics fall within a range of unstable frequencies

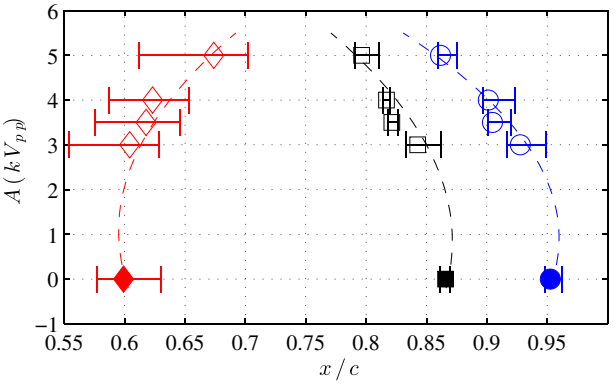

Fig. 6 The effect of excitation amplitude on the location of laminar separation (*red diamonds*), maximum bubble height (*black squares*), and reattachment (*blue circles*). Solid symbols denote baseline case. All forced cases pertain to $f^+ = 6$ (fitted trend lines are second-order polynomials). Error bars denote uncertainty interval

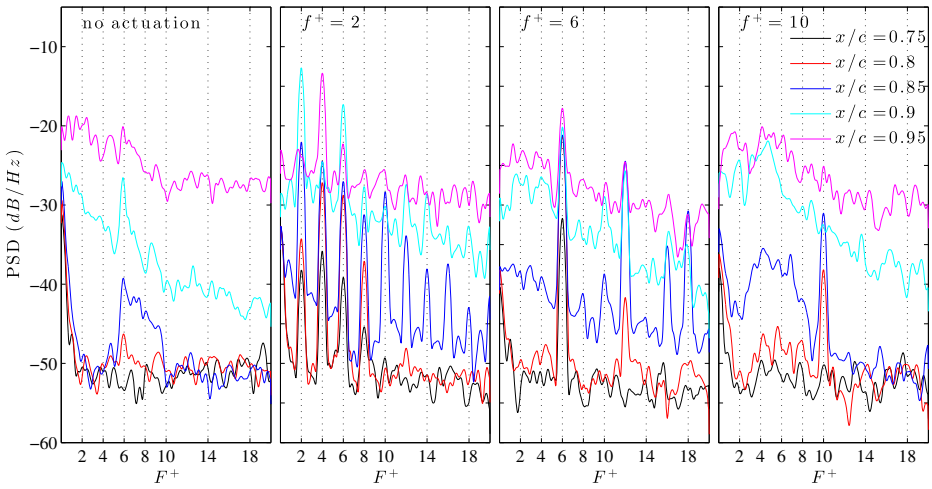

Fig. 7 Spectra of streamwise velocity fluctuations measured in the core of the separated shear layer (along the maxima in streamwise velocity fluctuations). For the controlled cases, the actuation is applied at 3.5 kV_{pp}. ($F^+ = Fc/U_\infty$)

in the baseline flow. Specifically, for $f^+ = 2$, the first and second harmonics fall within the unstable frequency range and are strongly amplified. In contrast, for $f^+ = 10$, a less significant amplification at the excitation frequency is attained. Instead, a broader band of unstable disturbances appears within the frequency range approximately matching that seen in the undisturbed flow. Consequently, while both excitation frequencies $f^+ = 2$ and $f^+ = 10$ are comparably separated from the fundamental frequency $F^+ \approx 6$, excitation at $f^+ = 2$ leads to a more significant diminishment of the separation bubble compared to that at $f^+ = 10$ (Figs. 4 and 5).

The changes brought about by the controlled disturbances to spatio-temporal dynamics of the laminar separation bubble are illustrated in Fig. 8, which depicts a series of instantaneous wall-normal velocity contours for the baseline and controlled case at $f^+ = 6$. The results show a distinct periodic pattern of positive and negative velocity, characteristic of a vortex train. Contours of λ_2 criterion [31] magnitude are shown by solid black lines in Fig. 8 to facilitate the identification of the vortices. The sequence of images confirms that the separated shear layer rolls up into periodic vortical structures upstream of the mean reattachment location for both cases shown in Fig. 8. These structures facilitate the entrainment of higher momentum fluid from the outer flow, re-energising the separated shear layer and leading to time-averaged flow reattachment. The flow development in the aft portion of the bubble is dominated by the shear layer vortices, and the time resolved bubble differs substantially from the time averaged bubble outline represented by mean dividing streamlines in Fig. 8 for convenience. Indeed, it can be argued that the notion of flow reattachment, as well as that of a separation bubble being a closed flow region, is a product of time-averaged flow field analysis. Applying the excitation at $f^+ = 6$ locks the amplified frequency band to the excitation frequency, which leads to earlier and more coherent shedding in the aft portion of the separation bubble than that seen for the baseline case.

To further quantify the effect of harmonic excitation on the temporal variation in the shedding frequency of the shear layer vortices, wavelet analysis was employed [32]. Analysis of velocity fluctuations measured in the aft portion of the separation bubble shear layer

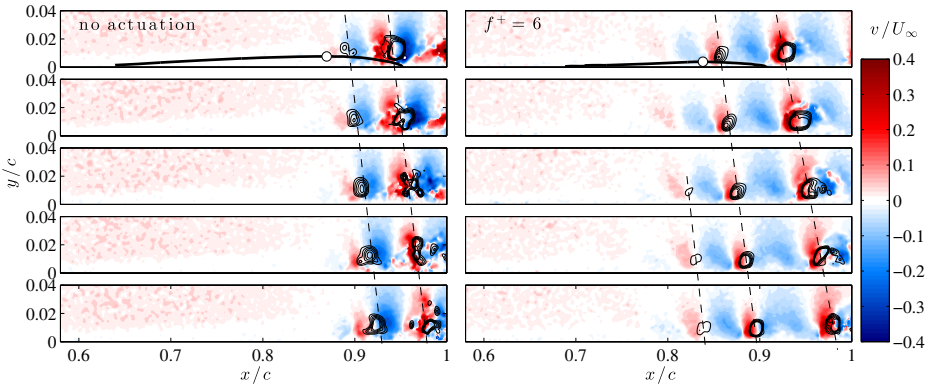

Fig. 8 Instantaneous contours of wall normal velocity (v) for cases of no actuation and excitation at $f^+ = 6$ and $A = 3.5kV_{pp}$. Each consecutive snapshot is separated by 0.5 ms. Contours of λ_2 criterion magnitude are shown to aid in vortex identification. Dashed lines connect the approximate streamwise position of separated shear layer vortices based on the local maxima in λ_2 magnitude. Thick solid black lines are the mean dividing streamlines, and circle markers identify the stramwise location the location of the maximum bubble height

was performed using a Morlet wavelet to characterise temporal changes in the frequency of the shear layer vortices (Fig. 9). For the baseline case, substantial temporal variations of the dominant frequency as well as amplitude are observed within the band of frequencies matching that of the amplified disturbances seen in Fig. 7. In contrast, when the flow is excited at $f^+ = 6$, the shedding frequency remains essentially steady at $F^+ = 6$. This is expected since shear layer disturbances lock onto the excitation frequency, as confirmed in the spectral results in Fig. 7, virtually eliminating any significant temporal variation in the shedding frequency.

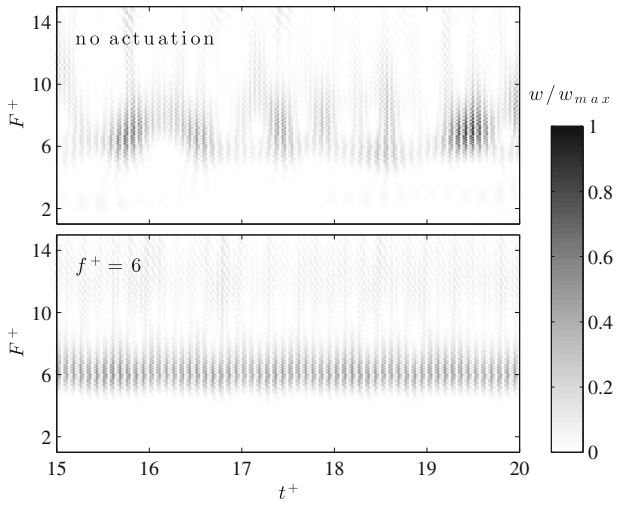

Fig. 9 Temporal variation of wavelet coefficients for the baseline case and $f^+ = 6$, $A = 3.5kV_{pp}$

Dashed lines in Fig. 8 trace the approximate streamwise positions of shear layer vortices in the images. The streamwise spacing between adjacent lines and the line slopes provide an indication of the streamwise wavelength and convective velocity of the structures, respectively. It can be seen that, despite the significant diminishment of the bubble produced by flow excitation, the convective velocity of the vortices near the roll-up location does not change substantially between the unexcited and excited cases, as can be seen from the similarity between the slopes of the most upstream dashed lines in Fig. 8. However, as the vortices propagate downstream, the convective velocity increases. Consequently, the streamwise wavelength at formation is comparable between the baseline and excited flow due to the similarity between shedding frequencies, but it tends to increase as the vortices develop downstream. The results in Fig. 8 also suggest that the roll-up vortices lose spatial coherence and start to breakdown in the redeveloping turbulent boundary layer, which is evidenced by the distortions in the periodic pattern in wall-normal velocity contours as well as the appearance of smaller scale structures identified by λ_2 contours. However, for the controlled case, this process is delayed. This implies that introducing artificial two-dimensional harmonic disturbances within the unstable frequency range delays the three dimensional breakdown of the structures discussed by Marxen et al. [18]. The attained effect is different from that observed by Jones et al [17], who used three-dimensional perturbations which appeared to promote the breakup of the main rollers. The ability of two-dimensional plasma actuation to enhance the coherence of dominant vortical structures has also been reported for other flows, e.g., for a cylinder wake by Benard and Moreau [33]. This signifies the importance of spanwise coherence and uniformity of introduced disturbances in the breakdown process of the LSB. In general, it appears that two-dimensional forcing pertinent to the plasma actuation used in this study enhances the coherence of roll-up vortices and delays turbulent breakdown.

To further analyse the effect of artificial disturbances on shear layer vortices, POD analysis was performed using the snapshot method [34]. Figure 10 shows the relative and cumulative modal energy distribution for the baseline case, continuous actuation at carrier frequency, and actuation at $f^+ = 6$. Evidently, the first two most energetic modes contain from about 20% to almost 40% of total energy for all the cases presented. These modes also contain comparable fraction of the total energy, suggesting that they are paired, as expected for flows dominated by strongly periodic structures [35, 36]. Applying continuous excitation reduces the energy content of the two most energetic modes from 27% to 20% and lowers the cumulative energy content of the first ten modes, suggesting that the same energy

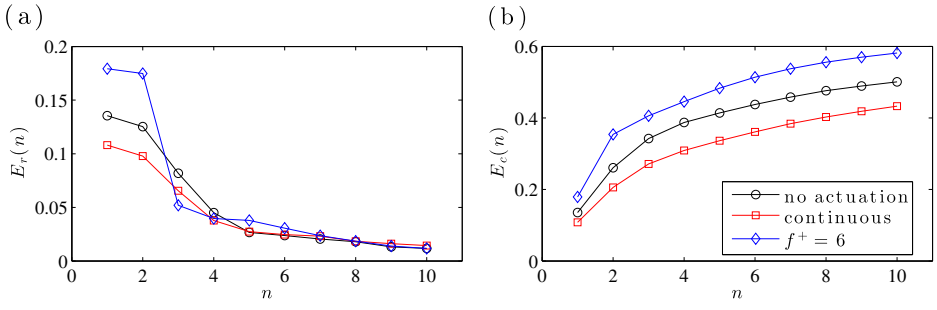

Fig. 10 Effect of excitation frequency on **(a)** relative modal energy distribution (E_r) and **b)** cumulative modal energy distribution (E_c) of POD modes. Excitation is applied at $A = 3.5kV_{pp}$

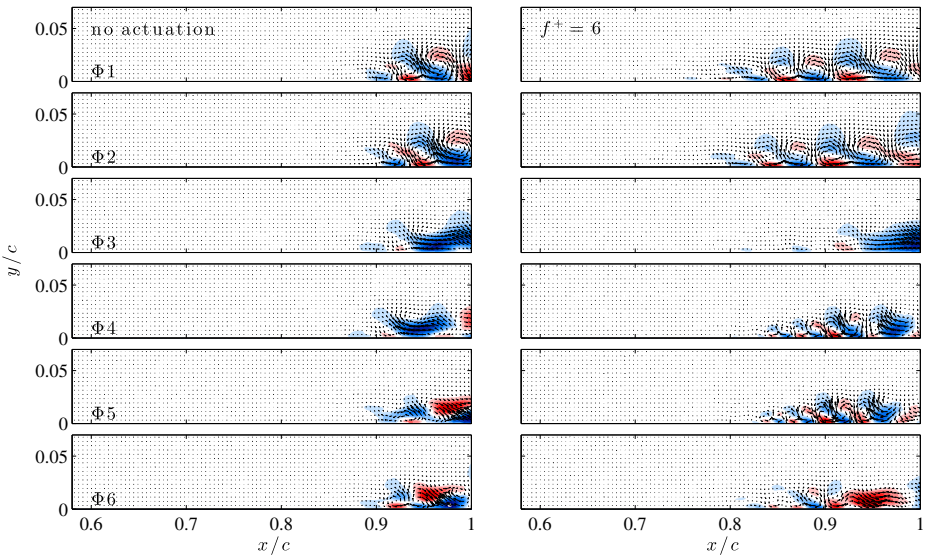

Fig. 11 Spatial POD modes coloured by the streamwise modal component for baseline and $f^+ = 6$, $A = 3.5kV_{pp}$ cases

content is being distributed over a wider range of modes. As discussed earlier, since the excitation is applied at a frequency much higher than the characteristic hydrodynamic frequencies in this case, the excitation simply acts to inject momentum to the boundary layer upstream of separation. This delays separation (Fig. 3) and also acts towards stabilising the boundary layer, leading to the reduction in the relative energy content of the most significant modes associated with shear layer disturbances. In contrast, when excitation is applied at $f^+ = 6$, the combined energy content of the first two modes increases from 27% in the baseline case to 37%. Since the excitation is applied at the frequency of naturally amplified disturbances, it promotes the growth of the most amplified disturbances, which are associated with the most energetic modes, producing the observed increase in the energy content of the first two modes.

The spatial POD modes are presented in Figs. 11 and 12, coloured by contours of the streamwise and wall-normal components, respectively. It can be seen that the first two modes feature a distinct periodic pattern of structures, characterised by the streamwise wavelength of the shear layer vortices (Fig. 8). These structures are spatially offset by a phase of $\pi/2$, as expected for the paired modes [36]. The spectra of the temporal coefficients presented in Fig. 13 confirm that the first two modes characterise strongly periodic velocity fluctuations associated with $F^+ = 6$, i.e., the frequency of shear layer vortices (Fig. 9). The results in Figs. 11–13 demonstrate that excitation can substantially affect the structure and characteristics of the higher modes. For the baseline case, sub-harmonic events in the shear layer are linked to modes 3 and 4 for the baseline case and mode 3 for the excited flow. Instead, periodic excitation energises harmonic content, dominant in modes 4, 5, and 6 in the excited flow (Fig. 13). The accompanying reduction in the energy content of the sub-harmonic modes in the excited flow case (Fig. 10) suggests that the sub-harmonic growth, common in separated shear layers [21], can be reduced by harmonic excitation at the fundamental frequency.

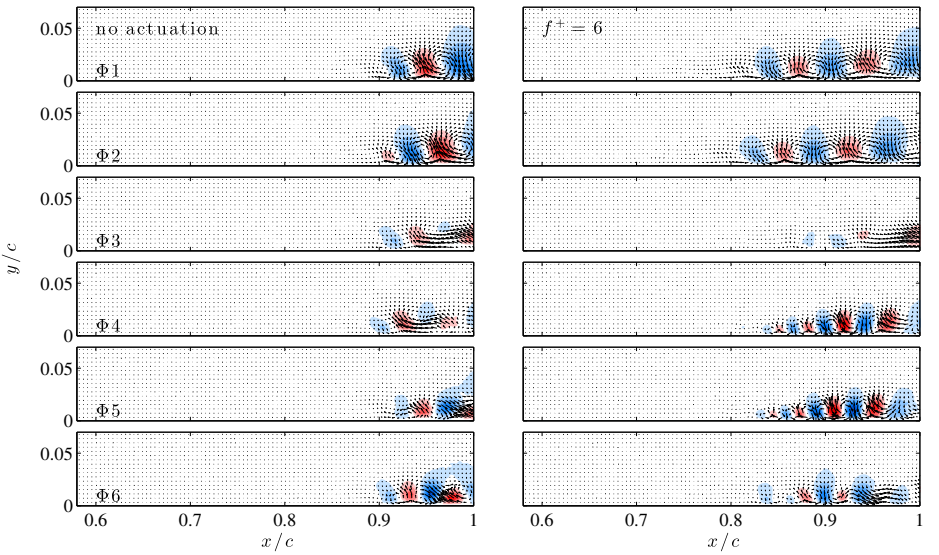

Fig. 12 Spatial POD modes coloured by the wall-normal modal component for baseline and $f^+ = 6$, $A = 3.5kV_{pp}$ cases

The effect of excitation amplitude on the modal energy distribution is presented in Fig. 14. The results confirm that, for the most cases examined, the introduction of harmonic disturbances at the frequency matching that of the naturally amplified disturbances acts to energise the first two modes that capture the dominant shear layer structures. As the amplitude is increased from $3kV_{pp}$ to $3.5kV_{pp}$, the energy content of the first two modes increases. However, further increase of the excitation amplitude decreases the relative energy content of these modes. For $A = 5kV_{pp}$, the energy content of modes 1 and 2 decreases below that in the baseline case. The changes in the relative energy content of the two primary modes are also accompanied by notable changes in the relative energy distribution of the lower modes. These observations suggest that the development of dominant disturbances must be influenced by other effects, which are speculated to be related to the diminishment of the separation bubble with increasing excitation amplitude (Fig. 6). Indeed, studies involving separated flows in the proximity of a solid boundary suggest that the

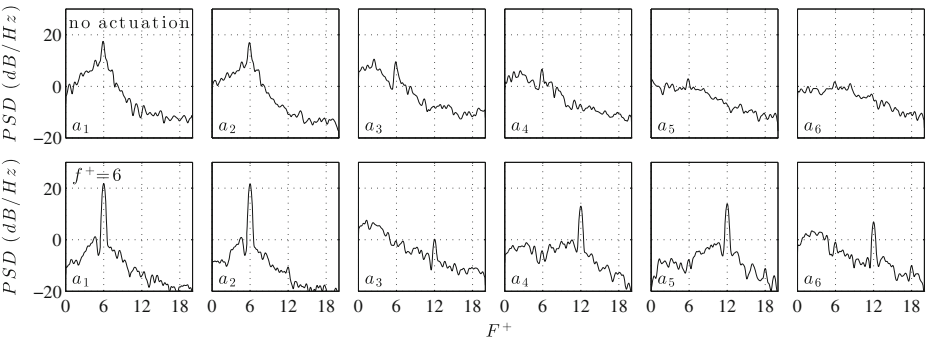

Fig. 13 Spectra of the temporal POD modes for baseline and $f^+ = 6$, $A = 3.5kV_{pp}$ cases

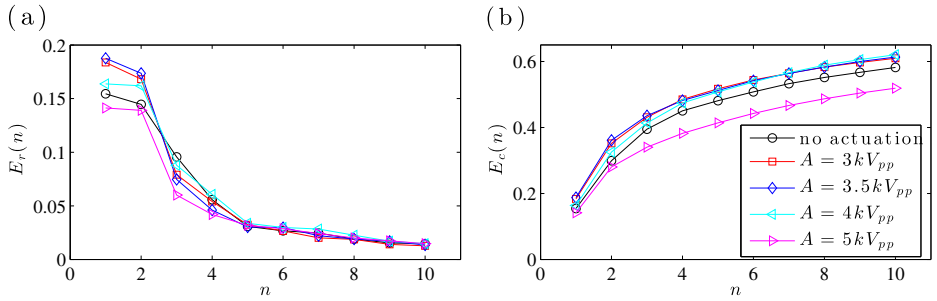

Fig. 14 Effect of excitation amplitude on **(a)** relative modal energy distribution (E_r) and **b)** cumulative modal energy distribution (E_c) of POD modes. Excitation is applied at $f^+ = 6$

proximity to the wall is a significant factor governing the development of disturbances in the shear layer [4, 7, 37] as well as the onset of non-linear interactions within the unstable wave packet [38], which is expected to affect the relative energy distribution of the POD modes related to fundamental, harmonic, and sub-harmonic growth.

The foregoing discussion shows that the optimal frequency of controlled disturbances correlates with the fundamental frequency of the amplified natural disturbances in unexcited flow. At the same time, excitation at the optimal frequency leads to significant deformation of the mean flow field (Fig. 3). Marxen & Henningson [7] and Marxen et al. [9] argue that such deformations can lead to changes in stability characteristics, which, if significant, would lead to changes in optimal excitation parameters. To relate the effect of artificial disturbances to stability characteristics of the separation bubble, linear stability theory (LST) analysis is applied to the investigated cases. The Orr-Sommerfeld equation for two dimensional flow was solved in spatial formulation assuming convective amplification of small amplitude disturbances in the separated shear layer using the measured time-averaged streamwise velocity profiles [39]. Note that the convective nature of the disturbance amplification is consistent with the experimental measurements, and the maximum reverse flow velocities are lower than the threshold required for the occurrence of a global instability [16].

While previous studies have shown the applicability of linear stability theory for predicting the essential characteristics of unstable disturbances in separation bubbles for both natural [13] and forced transition [9], it is first essential to validate the LST predictions and, more importantly, identify their limitations for the cases investigated. Fig. 15 shows a comparison of N factors [40] estimated from experimental measurements and LST predictions for the baseline case as well as for $f^+ = 6$, $A = 3.5kV_{pp}$. The N factor is defined for a disturbance of a given frequency as

$$N = \int_{x_0}^{x} -\alpha_i dx \tag{1}$$

where α_i is the growth rate of disturbances, x is the coordinate measured along the disturbance propagation direction, and x_0 is the neutral stability point, i.e., the most upstream x location where $\alpha_i = 0$. The N factor governs the growth of the amplitude of disturbances (A_d), as $A_d(x) = A(x_0)e^N$. For the purposes of comparing experimental data and LST predictions, the disturbance amplitude was extracted from experimental data as follows. The time resolved velocity field captured by PIV was bandpass filtered using a 6th degree Butterworth, zero phase lag digital filter. The bandpass filter of width of $\Delta F^+ = \pm 0.2$

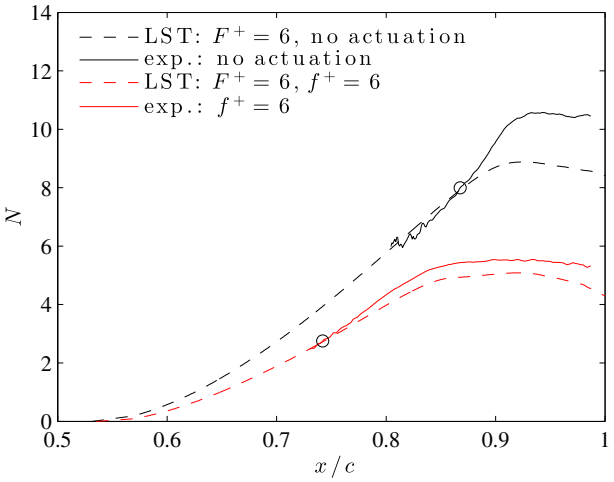

Fig. 15 Comparison of N factors from experiments and linear stability predictions for baseline case and the controlled case pertaining to $f^+ = 6$, $A = 3.5kV_{pp}$. The LST results are shown for $F^+ = 6$, while experimental data are filtered with a narrow bandpass filter centred at $F^+ = 6$. Black circles denote amplitude *match points* of $u' = 0.005U_\infty$

was centred at the desired frequency. Subsequently, the maximum of the rms of the filtered velocity field was extracted for each streamwise position. Due to the random noise of PIV measurements (≈1% of the instantaneous local velocities in the core of laminar separated shear layer ($\approx 0.01U_\infty$)), the amplitude of velocity fluctuations at the location of first instability ($A_d(x_0)$) cannot be resolved. As such, a reference *match point* between the experimentally-derived and LST-predicted N factors was used. The *match point* was selected at the streamwise location where the experimentally determined perturbation amplitude reached 0.5 % of the freestream velocity. The *match points* for the investigated cases are denoted with black circles in relevant figures.

The results presented in Fig. 15 show satisfactory agreement between experimental data and LST predictions. The convective amplification of disturbances is identified in the separated shear layer once disturbance amplitude exceeds the measurement noise level. The disturbances are then seen to be amplified nearly exponentially, suggesting essentially constant growth rate, similar to the results of Boutilier & Yarusevych [13]. This is followed by the gradual saturation of the disturbance growth, which can be deduced from the reduced rate of increase in the N factor. This occurs near the location of the maximum bubble height (Fig. 3). It is important to note that disturbances reach substantial amplitudes, which exceed the limit of approximately 1% of the freestream velocity beyond which linear approximations are often questioned [38]. However, LST predictions provide reliable predictions well above that limit, similar to the recent findings of Marxen et al. [9]. The agreement between N factors from experimental measurements and LST predictions is equally favourable for both the baseline case and forced case. This is of particular importance for the forced case, where initial amplitude of artificial disturbances substantially exceeds that in the baseline case. As will be shown later, the validity of LST predictions is also maintained at higher excitation amplitudes.

Figure 16 provides a comparison between disturbance profiles obtained from experimental data and those predicted by LST based on the data pertaining to the baseline and forced

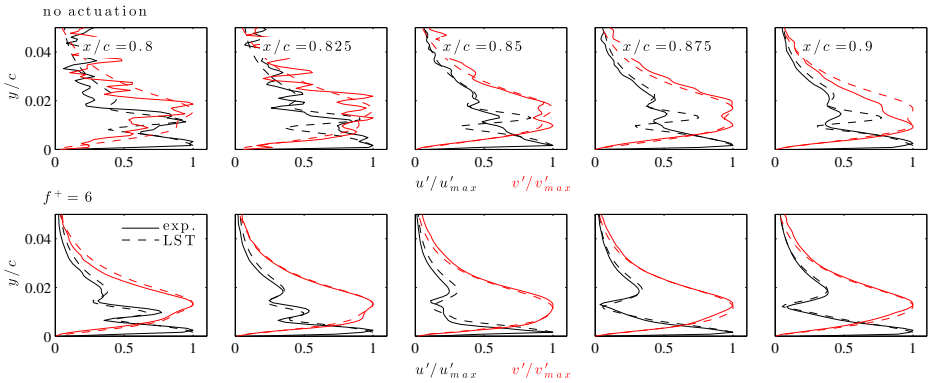

Fig. 16 Comparison of normalised disturbance profiles obtained from experiment and LST calculations for baseline case and the controlled case pertaining to $f^+ = 6$, $A = 3.5kV_{pp}$. The LST predictions are shown for $F^+ = 6$, while experimental data are bandpass filtered with a narrow bandpass filter centred at $F^+ = 6$

excitation at $f^+ = 6$, $A = 3.5kV_{pp}$. It can be seen that the experimental profiles agree well with LST results over the majority of the separation bubble length. In the fore portion of the bubble, random noise contaminates the experimental data in the baseline case, where disturbance amplitude is small. When the excitation is applied, the disturbance level increases and the disturbance profiles are well resolved in the same region. It is interesting to note that good agreement between experiments and LST is seen even in the aft portion of the bubble, particularly for the excited flow, where disturbance amplitudes $u' \approx 0.1U_\infty$ (Fig. 3). However, the agreement deteriorates as the reattachment location is approached, similar to the results in Fig. 15. Based on the present comparison it can be concluded that LST results can be used to infer stability characteristics of the separation bubble in the present investigation for both natural and forced transition.

Figure 17 presents contours of the local growth rate of disturbances (α_i) for the baseline case and forced case pertaining to $f^+ = 6$, $A = 3.5kV_{pp}$. The results pertaining to the baseline case demonstrate that past separation ($x/c = 0.6$), the highest growth rate (i.e., lowest α_i values) is associated with disturbances whose frequency $F^+ \approx 6$, agreeing with the spectral results in Fig. 7. When excitation is applied at $f^+ = 6$, separation occurs at $x/c = 0.68$ (Fig. 4). At and immediately downstream of these locations, the frequency associated with the highest growth rates remains close to the frequency of the most amplified disturbances in the undisturbed separation bubble ($F^+ \approx 6$). A comparison of the LST-predicted N factors between forced cases and the baseline case presented in Fig. 18 shows that, at a given streamwise location, the highest N factors are associated with $F^+ = 6$ for both the baseline case and all of the excitation frequencies. Thus, the excitation is most effective when its frequency matches this value, i.e., when forcing is applied at $f^+ = 6$. This analysis confirms the earlier speculation that the optimal excitation frequency is governed by stability characteristics of the separated shear layer.

In contrast to the relatively small effect on the excitation frequency, the results in Fig. 18 show that the maximum growth rate is reduced substantially for the forced case. This is also evidenced by the considerably lower N factors attained in the forced bubbles compared to those in the unforced bubble at all the excitation frequencies shown in Fig. 18. The most substantial reduction in the N factor is observed between the baseline case and forced cases, while less substantial deviations are observed between the forced cases. This decrease in the

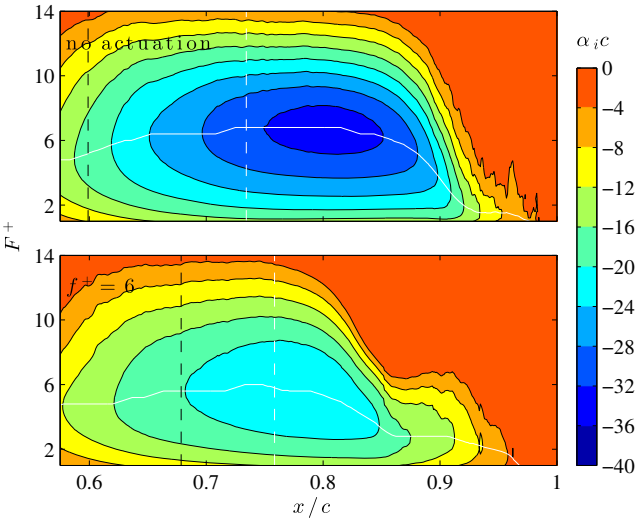

Fig. 17 LST stability curves based on the measured time-averaged velocity fields. For the controlled case ($f^+ = 6$) the actuation amplitude is $3.5kV_{pp}$. Solid white line denotes locus of most unstable frequencies. Dashed black and white lines denote location of separation and mid-position between separation and maximum bubble height locations, respectively

growth rate of disturbances is attributed to the reduction in the size of the separation bubble brought about by plasma forcing (Figs. 3–4). Dovgal et al. [4] show that the proximity of the separated shear layer to the wall can significantly affect the growth rates. Indeed, comparing the displacement thickness plots in Fig. 5 and the results in Fig. 18, it can be seen that, at a given streamwise location, the lower values of displacement thickness are associated with lower N factors. Note that the displacement thickness approximates the local wall normal distance between the wall and the separated shear layer [13]. Thus, the significant diminishment in the distance between the separated shear layer and the wall produced due to forcing (Fig. 5) correlates to a significant decrease in the N factors, and hence the growth rates of disturbances. At the same time, for this forcing amplitude, changes in excitation frequency produce much smaller changes in displacement thickness, which explains the smaller variation in the corresponding N factors.

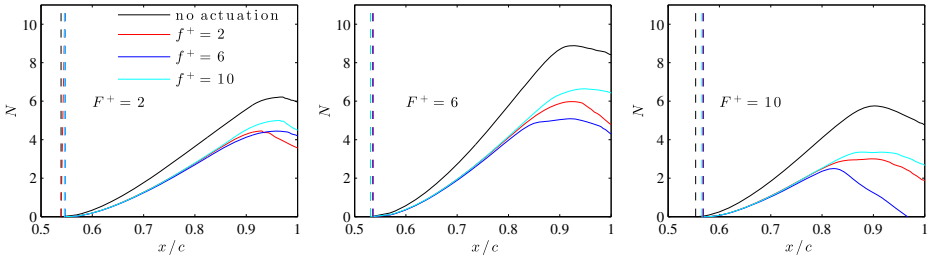

Fig. 18 N factors for frequencies of $F^+ = 2, 6, 10$, obtained from LST analysis.The forced cases pertain to the excitation amplitude of $A = 3.5kV_{pp}$. Dashed lines denote location of first instability (x_0) for the respective mode

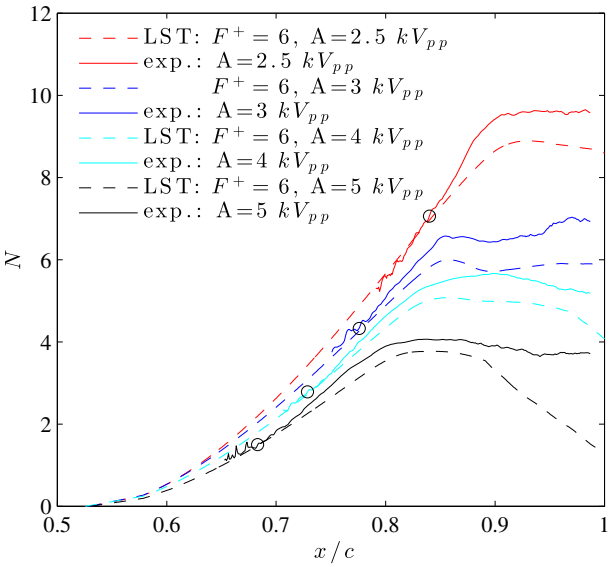

Fig. 19 N factors pertaining to different excitation amplitudes applied at $f^+ = 6$. The experimental data were bandpass filtered at $F^+ = 6$. Black circles denote amplitude *match points* of $u' = 0.005U_\infty$

The effect of excitation amplitude on the N factor for harmonic disturbances applied at $f^+ = 6$ is shown in Fig. 19. The close agreement between the LST predictions and experimental data further confirms the applicability of linear stability analysis even at the highest excitation amplitudes tested in the present investigation. The results demonstrate that, at a given streamwise position, the increase in excitation amplitude reduces the N factor, which implies the reduction in the average growth rate of the disturbances. As discussed earlier, this is associated with the diminishment of the separation bubble (Fig. 6), and the associated decrease in the distance between the separated shear layer and the wall.

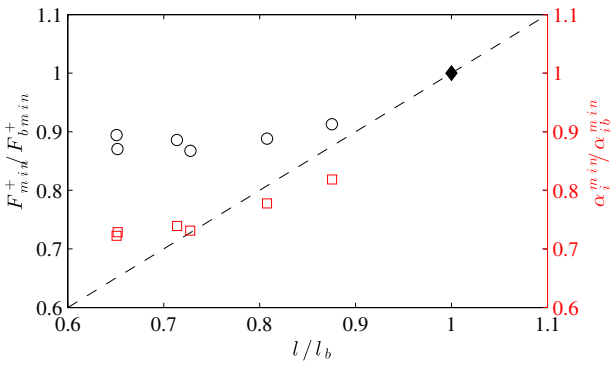

Fig. 20 Variation of the frequency of the most amplified disturbances and the minimum growth rate with length of separation bubble. All parameters are normalised by the values pertaining to the baseline case *(black diamond)*

The variation of the frequency of the most amplified disturbances and the growth rate with the reduction in the size of the separation bubble is presented in Fig. 20 for all the cases examined here. All data are normalised by the values pertaining to the baseline case. The results confirm that the diminishment of the bubble is associated with a moderate decrease in the frequency of the most amplified disturbances. Specifically, a reduction of the bubble length by about 35% leads to a reduction of the most amplified frequency by about 10%. The implication here is that the mean flow deformation induced by controlled local flow excitation does not substantially affect the frequency of the most amplified disturbances in the separation bubble. This conclusion is supported by the results of Yarusevych et al. [19], where optimal frequency of acoustic excitation matched the fundamental frequency in the unexcited flow to within about 10% for the majority of the cases examined. Moreover, considering recent numeric results of Marxen et al. [9], the variations observed in the frequency associated with the most amplified disturbances in a separation bubble are also relatively small compared to the degree of deformation of the mean bubble induced by the simulated synthetic jet actuation. It should be noted, however, that improvements in control authority can be gained for a given excitation amplitude by adjusting the excitation frequency to account for flow deformations, which agrees with numerical simulations of Marxen et al. [9]. For example, additional contraction of the separation bubble may be achieved by reducing the excitation frequency of $f^+ = 6$ to match that of the most amplified disturbances in the depressed bubble. The present data also show that the decrease in the most amplified frequency appears to diminish as the size of the bubble is decreased by excitation.

In comparison to the changes in the frequency of the most amplified disturbances, the maximum growth rate diminishes more substantially as the bubble length decreases. The decrease in bubble length of approximately 35% leads to the decrease in the growth rate by almost 30%. The results suggest that the decrease in the maximum growth rate is roughly linearly proportional to the decrease in the length of the bubble, but the trend is altered for $l/l_b < 0.7$, where the decrease in the growth rate begins to saturate. From their numerical simulations, Marxen & Henningson [7] and Marxen et al. [9] also report substantial decrease in growth rates due to mean flow deformation.

The present results of the linear stability analysis provide insight into the mechanism of the frequency selection for optimal harmonic excitation of the laminar separation bubble. The data also quantified the effect of mean flow deformation on the stability characteristics. When the separation bubble is diminished by harmonic forcing, the frequency of the most amplified disturbances decreases. Although the decrease is moderate relative to the degree of mean flow deformation, this is an important finding since the trend is perhaps counter intuitive from the perspective of global scaling, where shorter length scales of the bubble typically imply higher fundamental frequencies in undisturbed flows. This is also of interest for improving the efficiency of flow control by adjusting the frequency of excitation to match that of the most unstable disturbance. It is important to note that the diminishment of the bubble leads to the decrease in the growth rate of the most amplified disturbances. However, the bubble size is reduced in the first place due to the advancement of transition through the introduction of controlled disturbances. This implies that disturbances must be amplified to critical amplitudes required for the shear layer to roll up and shed vortices earlier upstream. Considering the relation between disturbance amplitudes and the N factor, $A_d(x) = A_d(x_0)e^N$, earlier roll-up is achieved due to the increase in the initial amplitude of the disturbances despite the diminishment in the N factor. This competing effect of bubble becoming more stable with increasing excitation amplitudes may be responsible for the decreased response of the bubble to the increase in excitation amplitude (Fig. 6). Finally, the

significant variation in flow stability between the unperturbed bubble and that attained by means of controlled forcing suggests a potential significance of the initial, transient response of the bubble to the introduction of controlled disturbances, which may influence the final quasi-steady characteristics of the bubble attained by continuous excitation.

4 Conclusions

The effect of controlled local disturbances on flow development and stability of a laminar separation bubble has been investigated experimentally on a NACA 0012 airfoil at $\alpha = 2°$ and $Re_c = 130\,000$. The disturbances were introduced upstream of separation by means of a surface mounted DBD plasma actuator. The effect of excitation frequency and amplitude on flow characteristics has been investigated. The flow field has been characterised by means of time-resolved, two-component PIV measurements, allowing capturing changes in spatio-temporal flow development.

The results demonstrate that the introduction of periodic disturbances leads to the reduction in the size of the separation bubble. The most significant effect is produced when excitation is applied at the frequency matching the frequency of the most amplified disturbances i.e., the fundamental frequency. The introduced disturbances and their harmonics are amplified in the separated shear layer, with the strongest amplification occurring at the fundamental frequency. The amplification of disturbances leads to shear layer roll-up and shedding of shear layer vortices. POD analysis confirmed that these are the most energetic structures, which govern flow development in the aft portion of the bubble. The shedding of these structures leads to flow reattachment in the mean sense. Thus, forcing the flow at the fundamental shear layer frequency leads to earlier shear layer roll up and the upstream advancement of the mean reattachment location. The associated changes in the flow field also lead to a delayed separation, producing an overall decrease in the extent of the separation bubble. Increasing the amplitude of the introduced disturbances enhances this effect.

The linear stability theory analysis has showed good agreement with experimental measurements, even in the aft portion of the bubble where disturbances reach significant amplitudes. The results demonstrate that significant mean flow deformation produced due to the introduction of controlled disturbances affects stability characteristics. The frequency of the most amplified disturbances is found to decrease with decreasing size of the bubble brought about by controlled forcing. However, the decrease is rather small compared to the degree of flow deformation. While the length of the separation bubble was decreased by about 35%, the fundamental frequency decreased by about 10%. This suggests that the frequency of the most unstable disturbances in the unperturbed flow can provide a reasonable estimate for the optimal excitation frequency, which confirms empirical results of previous studies [19].

The diminishment in the size of the bubble by controlled excitation also decreases the maximum growth rate and N factors. The effect of mean flow deformation is much more substantial compared to that on the fundamental frequency, with maximum growth rates decreasing by almost 30%. This effect is correlated to the decrease in the distance between the separated shear layer and the wall, with the proximity of the wall dampening the growth of disturbances. The associated decrease in the N factor implies that the upstream advancement of shear layer roll up, required for the diminishment of the bubble, is achieved due to higher initial amplitude of the perturbation introduced by the actuator. The diminishment of the separation bubble produced by the increase in the excitation amplitude is thus countered

by the increasing stability of the bubble. This is expected to lead to the eventual saturation of the control authority, as long as the actuator itself does not directly produce significant changes to the mean flow field.

Acknowledgments The authors gratefully acknowledge the Natural Sciences and Engineering Research Council of Canada (NSERC Discovery Grant #112539) and TU Delft for funding this work.

References

1. Carmichael, B.H.: Low reynolds number airfoil survey NASA CR 165803 (1981)
2. Gaster, M.: The Structure and Behaviour of Laminar Separation Bubbles Reports and Memoranda, vol. 3595. Aeronautical Research Council, London (1967)
3. Burgmann, S., Schröder, W.: Investigation of the vortex induced unsteadiness of a separation bubble via Time-Resolved and scanning PIV measurements. Exp. Fluids **45**(4), 675–691 (2008)
4. Dovgal, A., Kozlov, V., Michalke, A.: Laminar boundary layer separation: Instability and associated phenomena. Prog. Aerosp. Sci. **30**, 61–94 (1994)
5. Hain, R., Kähler, C.J., Radespiel, R.: Dynamics of laminar separation bubbles at Low-Reynolds-Number aerofoils. J. Fluid Mech. **630**, 129 (2009)
6. Jones, L.E., Sandberg, R.D., Sandham, N.D.: Stability and receptivity characteristics of a laminar separation bubble on an aerofoil. J. Fluid Mech. **648**, 257–296 (2010)
7. Marxen, O., Henningson, D.S.: The effect of Small-Amplitude convective disturbances on the size and bursting of a laminar separation bubble. J. Fluid Mech. **671**, 1–33 (2011)
8. Gad-el Hak, M.: Flow control: The future. J. Aircr. **38**(3), 402–418 (2001)
9. Marxen, O., Kotapati, R.B., Mittal, R., Zaki, T.: Stability analysis of separated flows subject to control by zero-net-mass-flux jet. Phys. Fluids (1994-present) **27**(2), 024107 (2015)
10. Postl, D., Balzer, W., Fasel, H.F.: Control of laminar separation using pulsed vortex generator jets: Direct numerical simulations. J. Fluid Mech. **676**, 81–109 (2011)
11. Yarusevych, S., Sullivan, P.E., Kawall, J.G.: Effect of acoustic excitation amplitude on airfoil boundary layer and wake development. AIAA J. **45**(4), 760–771 (2007)
12. Tani, I.: Low-Speed Flows involving bubble separations. Prog. Aerosp. Sci. **5**, 70–103 (1964)
13. Boutilier, M.S.H., Yarusevych, S.: Separated shear layer transition over an airfoil at a low Reynolds number. Phys. Fluids **24**(8), 084105 (2012)
14. Häggmark, C.P., Hildings, C., Henningson, D.S.: A numerical and experimental study of a transitional separation bubble. Aerosp. Sci. Technol. **5**(5), 317–328 (2001)
15. Lang, M., Rist, U., Wagner, S.: Investigations on controlled transition development in a laminar separation bubble by means of LDA and PIV. Exp. Fluids **36**(1), 43–52 (2004)
16. Alam, M., Sandham, N.D.: Direct numerical simulation of short laminar separation bubbles with turbulent reattachment. J. Fluid Mech. **410**, 223–250 (2000)
17. Jones, L.E., Sandberg, R.D., Sandham, N.D.: Direct numerical simulations of forced and unforced separation bubbles on an airfoil at incidence. J. Fluid Mech. **602**, 175–207 (2008)
18. Marxen, O., Lang, M., Rist, U.: Vortex formation and vortex breakup in a laminar separation bubble. J. Fluid Mech. **728**, 58–90 (2013)
19. Yarusevych, S., Kawall, J.G., Sullivan, P.E.: Airfoil performance at low reynolds numbers in the presence of periodic disturbances. J. Fluids Eng., Transactions of the ASME, **128**(3), 587–595 (2006)
20. Yarusevych, S., Sullivan, P.E., Kawall, J.G.: Coherent structures in an airfoil boundary layer and wake at low Reynolds numbers. Phys. Fluids **18**(4), 044101 (2006)
21. Yarusevych, S., Sullivan, P.E., Kawall, J.G.: On vortex shedding from an airfoil in Low-Reynolds-Number flows. J. Fluid Mech. **632**, 245–271 (2009)
22. Ol, M.V., Mcauliffe, B.R., Hanff, E.S., Scholz, U., Kähler, C.: Comparison of laminar separation bubble measurements on a low Reynolds number airfoil in three facilities. In: 35th AIAA Fluid Dynamics Conference and Exhibit, June, Toronto (2005)
23. Greenblatt, D., Wygnanski, I.J.: Control of flow separation by periodic excitation. Prog. Aerosp. Sci. **36**(7), 487–545 (2000)
24. Rizzetta, D.P., Visbal, M.R.: Numerical investigation of plasma-based control for low-reynolds-number airfoil flows. AIAA J. **49**(2), 411–425 (2011)

25. Boutilier, M.S.H., Yarusevych, S.: Effects of end plates and blockage on low-reynolds-number flows over airfoils. AIAA J. **50**(7), 1547–1559 (2012)
26. Pröbsting, S., Yarusevych, S.: Laminar separation bubble development on an airfoil emitting tonal noise. J. Fluid Mech. **780**, 167–191 (2015)
27. Wieneke, B.: PIV uncertainty quantification from correlation statistics. Meas. Sci. Technol. **26**, 074002 (2015)
28. Burgmann, S., Dannemann, J., Schröder, W.: Time-Resolved and volumetric PIV measurements of a transitional separation bubble on an SD7003 airfoil. Exp. Fluids **44**(4), 609–622 (2008)
29. Kotsonis, M., Ghaemi, S., Veldhuis, L., Scarano, F.: Measurement of the body force field of plasma actuators. J. Phys. D Appl. Phys. **44**(4), 045204 (2011)
30. Kotsonis, M.: Diagnostics for characterisation of plasma actuators. Meas. Sci. Technol. **26**(9), 092001 (2015)
31. Jeong, J., Hussain, F.: On the identification of a vortex. J. Fluid Mech. **285**, 69–94 (1995)
32. Torrence, C., Compo, G.P.: A practical guide to wavelet analysis. Bull. Am. Meteorol. Soc. **79**(1), 61–78 (1998)
33. Benard, N., Moreau, E.: Response of a circular cylinder wake to a symmetric actuation by non-thermal plasma discharges. Exp. Fluids **54**, 1467 (2013)
34. Sirovich, L., Kirby, M.: Low-dimensional procedure for the characterization of human faces. J. Opt. Soc. Am. A Opt. Image Sci. **4**(3), 519–524 (1987)
35. Lengani, D., Simoni, D., Ubaldi, M., Zunino, P.: POD analysis of the unsteady behavior of a laminar separation bubble. Exp. Thermal Fluid Sci. **58**, 70–79 (2014)
36. Oudheusden, B., Scarano, F., Hinsberg, N., Watt, D.: Phase-resolved characterization of vortex shedding in the near wake of a square-section cylinder at incidence. Exp. Fluids **39**(1), 86–98 (2005)
37. Diwan, S.S., Ramesh, O.N.: On the origin of the inflectional instability of a laminar separation bubble. J. Fluid Mech. **629**, 263–298 (2009)
38. Boiko, A., Dovgal, A., Hein, S., Henning, A.: Particle image velocimetry of a Low-Reynolds-Number separation bubble. Exp. Fluids **50**(1), 13–21 (2011)
39. Van Ingen, J., Kotsonis, M.: A Two-Parameter Method for En Transition Prediction. In: 6th AIAA Theoretical Fluid Mechanics Conference (2011)
40. Drazin, P.G., Reid, W.H.: Hydrodynamic stability (1981)